Draft version July 14, 2004
Preprint typeset using LaTeX style emulateapj v. 6/22/04

FORMATION OF GLOBULAR CLUSTERS IN GALAXY MERGERS

Yuexing Li, Mordecai-Mark Mac Low
Department of Astronomy, Columbia University, New York, NY 10027, USA and
Department of Astrophysics, American Museum of Natural History, 79th Street at Central Park West, New York, NY 10024-5192, USA
and
Ralf S. Klessen
Astrophysikalisches Institut Potsdam, An der Sternwarte 16, D-14482 Potsdam, Germany
Draft version July 14, 2004

ABSTRACT

We present a high-resolution simulation of globular cluster formation in a galaxy merger. For the first time in such a simulation, individual star clusters are directly identified and followed on their orbits. We quantitatively compare star formation in the merger to that in the unperturbed galaxies. The merging galaxies show a strong starburst, in sharp contrast to their isolated progenitors. Most star clusters form in the tidal tails. With a mass range of 5×10^5–$5 \times 10^6 M_\odot$, they are identified as globular clusters. The merger remnant is an elliptical galaxy. Clusters with different mass or age have different radial distributions in the galaxy. The cluster mass spectrum appears to be roughly log-normal. Our results show that the high specific frequency and bimodal distribution of metallicity observed in elliptical galaxies are natural products of gas-rich mergers, supporting a merger origin for the ellipticals and their globular cluster systems.

Subject headings: galaxy: interactions — galaxy: globular clusters — galaxy: star formation — galaxy: evolution — star clusters: formation

1. INTRODUCTION

Galaxy interactions and mergers are among the most spectacular shows on the stage of the hierarchical universe. They are pivotal elements of cosmic structure formation and evolution. In the past decade, the Hubble Space Telescope (HST) has unveiled evidence for the formation of massive star clusters or young globular clusters in merging galaxies, such as NGC 7252 (Whitmore et al. 1993), the Antennae Galaxy (Whitmore & Schweizer 1995), NGC 3597 (Holtzman et al. 1996), and NGC 3921 (Schweizer et al. 1996), see Whitmore (2001) for a review.

Several theoretical models for the formation of globular clusters (GCs) and GC systems have been proposed, such as primary models where clusters form before galaxies (e.g Peebles & Dicke 1968), secondary models where clusters form with galaxies (e.g. Fall & Rees 1985; Harris & Pudritz 1994), tertiary models where clusters form after galaxies, such as in mergers (Ashman & Zepf 1992), and unified models (Elmegreen & Efremov 1997). See Harris (1991); Ashman & Zepf (1998) and Carney & Harris (2001) for comprehensive reviews. In particular the merger-induced formation scenario has been galvanized by the HST observations. There have been many numerical simulations of galaxy mergers (Toomre & Toomre 1972; White 1978; Farouki & Shapiro 1982; Barnes & Hernquist 1992; Hernquist 1992; Mihos & Hernquist 1994, 1996; Dubinski et al. 1999; Springel & White 1999; Springel 2000; Naab & Burkert 2001; Barnes 2002), but only a few calculations focus on GC formation in mergers. These include semi-analytical models (Beasley et al. 2002), combined N-body and smoothed particle hydrodynamics (SPH) simulations (Bekki & Chiba 2002; Bekki et al. 2002), and extended cosmological simulations by Kravtsov & Gnedin (2003). In these models individual GCs are not identified and directly followed. In addition, the star formation history of the merger is not compared to that of the isolated progenitors.

We here model GC formation in both isolated disk galaxies and their mergers using high resolution, three-dimensional, SPH simulations. We use absorbing sink particles to directly represent individual massive young star clusters. In § 2 we briefly describe our computational method. We discuss the burst of GC formation during the merging event in § 3, and compare with the evolution of the isolated galaxy. We then focus on the cluster mass and age distribution at the end of the merger in § 4, and discuss the mass spectrum of clusters formed at different epochs in § 5. We summarize in §6.

2. NUMERICAL METHOD

The numerical method is described in detail in Li et al. (2004). We use the publicly available SPH code GADGET (Springel et al. 2001), and implement absorbing sink particles that do not interact hydrodynamically (Bate et al. 1995) to directly measure the mass of gravitationally collapsing gas. To represent GCs, we allow sinks to form from regions where the local density exceeds 1000 cm^{-3} (Bromm & Clarke 2002). Our galaxy model consists of a dark matter halo, and a disk of stars and isothermal gas. We follow the analytical work by Mo et al. (1998) and the numerical implementation by Springel & White (1999) and Springel (2000). Our simulations meet three numerical criteria, the Jeans resolution criterion (Bate & Burkert 1997), the gravity-hydro balance criterion for gravitational softening (Bate & Burkert 1997), and the equipartition criterion for particle masses (Steinmetz & White 1997). We adopt a halo concentration parameter $C = 5$, a spin parameter $\lambda = 0.05$, and Hubble constant $H_0 = 70$ km s^{-1} Mpc^{-1} (Springel 2000).

Electronic address: yxli@astro.columbia.edu, mordecai@amnh.org, rklessen@aip.de

The galaxy model studied here (G100-1 in Li et al. 2004) initially has rotational velocity $V_{200} = 100$ km s^{-1} at the virial radius where the overdensity is 200, and a virial mass of $M_{200} = 3.3 \times 10^{11} M_\odot$. Total mass in the disk and in the disk gas as fraction of the virial mass are $f_{\rm d} = 0.05$ and $f_{\rm g} = 0.01$, respectively. An isothermal equation of state with sound speed $c_{\rm s} = 6$ km s^{-1} is used. The total particle number for each single galaxy is $N_{\rm tot} = 1 \times 10^6$, with $N_{\rm g} = 5 \times 10^5$, $N_{\rm d} = 2 \times 10^5$, and $N_{\rm h} = 3 \times 10^5$ for disk gas and stars, and halo dark matter, respectively. The corresponding gravitational softening lengths are $\epsilon_{\rm g} = 0.01$, $\epsilon_{\rm d} = 0.1$, and $\epsilon_{\rm h} = 0.4$ kpc. The spatial resolution of gas is 10 pc, and the mass per gas particle is $6.6 \times 10^3 M_\odot$. Compared to Bekki et al. (2002) this improves the resolution by two orders of magnitude.

We perform two simulations. One follows the evolution of the isolated galaxy described above, and the other is an equal-mass, head-on merger of two such galaxies. The two galaxies are on a parabolic orbit and are separated initially by a distance of 150 kpc. In the merger run, $N_{\rm tot} = 2 \times 10^6$, with $N_{\rm g} = 1 \times 10^6$ gas particles and corresponding other particle numbers. The simulations are followed for up to 5 Gyr.

3. STARBURSTS IN THE MERGING EVENT

3.1. *Where Do Globular Clusters Form?*

Our single galaxy is a marginally stable model in which stars form slowly but steadily, and most of the clusters form in the central region, as described by Li et al. (2004). In the merging event, sporadic star formation occurs during the approach phase in the central region of each galaxy. The first close encounter occurs at $t \sim 1.4$ Gyr. The galaxies then separate to a distance of about 100 kpc at $t \sim 2$ Gyr, fall back, and finally merge at $t \sim 4.5$ Gyr. There are vigorous starbursts in each of the two close encounters.

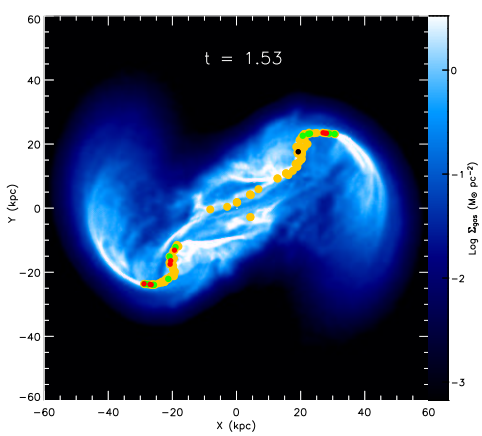

FIG. 1.— Globular clusters formed in the merger. The blue-white image is the gas surface density at $t = 1.53$ Gyr, with values given by the color bar. The colored dots represent (*yellow*) older GCs with lifetimes $\tau_{\rm gc} > 10$ Myr, (*green*) young GCs with $\tau_{\rm gc} < 10$ Myr and $M_{\rm gc} < 10^6 M_\odot$, (*red*) young GCs with $M_{\rm gc} \geq 10^6 M_\odot$, and (*black*) the most massive young GC.

Most clusters form during the first close encounter at t =1.4–1.7 Gyr. Their mass range spans $5 \times 10^5 M_\odot$ to $5 \times 10^6 M_\odot$, where we assume a local star formation efficiency of 35%. We therefore identify these clusters as newly formed GCs. However, sink particles do not lose mass from dynamical effects as real GCs do, so this identification should be used cautiously.

Figure 1 shows a snapshot in the middle of the first encounter at t =1.53 Gyr. GCs form in the extended tidal tails and bridges where the gas reaches high density. The derived mass range agrees well with spectroscopic estimates by Mengel et al. (2002) of some young clusters in the Antennae Galaxy, and the morphology of the distribution is very similar to the observation that most of the clusters there form in tidal tails and bridges (Whitmore & Schweizer 1995; Zhang et al. 2001).

3.2. *Comparison Between Merger and Isolated Galaxy*

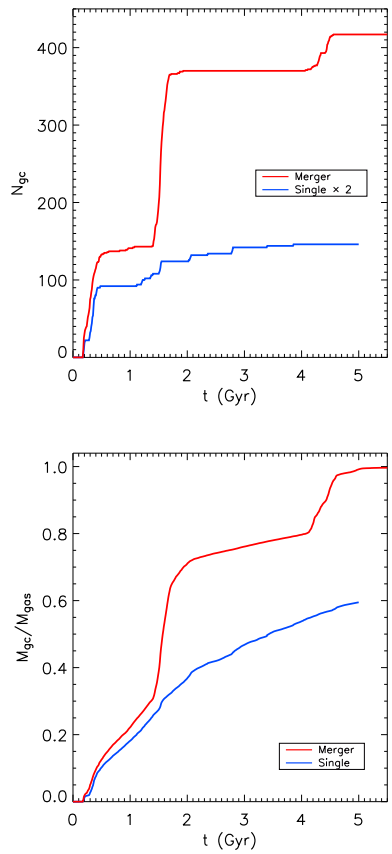

FIG. 2.— Number $N_{\rm gc}$ (*top*) and mass $M_{\rm gc}/M_{\rm gas}$ (*bottom*) of GCs over time compared between two merging galaxies (*red lines*) and two isolated galaxies (*blue lines*). Note the sudden jumps in the merging galaxies, representing starbursts.

Figure 2 compares star formation in the isolated galaxy with the galaxy merger. In the isolated galaxy, stars start to form at $t \sim 0.3$ Gyr when gas density increases because of gravitational instability in the disk. The cluster number $N_{\rm gc}$ increases slowly as the galaxy maintains marginal stability (Li et al. 2004), reaching only 73 in the end. In the merging event, the gas density is increased vastly by shocks and tidal forces, leading to starbursts. Cluster formation rate $dM_{\rm gc}/dt$ and $N_{\rm gc}$ increase dramatically. Rapid growth starts at $t \sim 1.4$ Gyr during

the first encounter, and again at $t \sim 4$ Gyr in the second encounter. However, the effect is stronger in the first encounter because more gas is available for star formation. The merger produces 417 GCs.

The specific frequency (Harris & van den Berg 1981) of GCs in a galaxy $S_{\rm N} = N_{\rm t} 10^{0.4(\mathcal{M}_{\rm v}+15)}$, where $N_{\rm t}$ is the total number of GCs, and the V-band absolute magnitude of the host galaxy, $\mathcal{M}_{\rm v} = \mathcal{M}_{\odot} - 2.5\log(L_{\rm v}/L_{\odot})$. We use the method of Bekki et al. (2002) to estimate $S_{\rm N}$ in our models. If we assume a mass loss rate of 50% for the total stars, and a cluster survival rate of 50% for the GCs, then the single galaxy has a final stellar mass of $M_* \sim 7 \times 10^9 M_{\odot}$. Assuming a mass-to-light ratio of 3, we can derive $\mathcal{M}_{\rm v} \sim -18.7$ mag, so $S_{\rm N} \sim 1.2$. Similarly, the elliptical merger remnant has $M_* \sim 1.5 \times 10^{10} M_{\odot}$, which gives $\mathcal{M}_{\rm v} \sim -19.5$ mag, so $S_{\rm N} \sim 3.3$. These values are consistent with observations. For example, the Milky Way-like spiral M31 has $S_{\rm N} \sim 1.2 \pm 0.2$ (Barmby & Huchra 2001), while typical ellipticals have $S_{\rm N} \sim 3.5$ (Harris 1991; McLaughlin 1999). These estimates do depend on the mass-to-light ratio (e.g. Larsen et al. 2002) and survival rate of the clusters (Fall & Zhang 2001; Whitmore 2004). Nevertheless, they reflect the difference between isolated disk galaxies and mergers, and suggest that mergers can explain the considerably higher specific frequency of GCs observed in elliptical galaxies.

4. MERGER REMNANT

Star formation during the merger leads to rapid gas depletion. By $t = 5$ Gyr the two merging galaxies have transformed into an elliptical galaxy, as is shown in Figure 3. Three distinct populations of GCs form at different epochs, as shown in the Figure. GCs formed during the two close encounters are almost coeval, as they form over a very short period during the encounters.

GCs with different mass or age have different radial distributions. Massive GCs are centrally concentrated, while less massive ones extend further out. Both the old GCs formed prior to the first encounter, and the youngest GCs formed in the second encounter are centrally concentrated. The oldest GCs in our simulation are also the most massive, and quickly sink towards the center by dynamical friction. The youngest ones are formed in the galactic center because remaining gas assembles there during the final merger. The majority of GCs from the first encounter, however, spread out to more than 20 kpc, because they form in the tidal tails and have large angular momentum.

If we assume a metallicity-age relation such that older GCs have lower metallicities (Rich, Shara & Zurek 2001), we clearly see a bimodal metallicity distribution. Young, high-metallicity GCs are centrally concentrated, while older, lower-metallicity GCs extend to larger radii, in agreement with observations (Djorgovski & Meylan 1994). The isolated galaxy forms clusters slowly and steadily, so age, as well as metallicity, follow a smooth distribution. There is no bimodality. Our results thus support the arguments of Ashman & Zepf (1992) and Kundu & Whitmore (2001) that mergers are required to produce a bimodal distribution.

5. GLOBULAR CLUSTER MASS SPECTRUM

One of the most important characteristics of old ($\sim$ 10 Gyr) globular clusters is their universal Gaussian luminosity distribution function (or mass function), which makes them standard candles. Recently, it has been suggested that the mass functions of *young* GCs can be approximated by a power-law $dN/dM \propto M^{-\alpha}$ with α = 1.5–2 (Harris & Pudritz 1994; Elmegreen & Efremov 1997). Zhang & Fall (1999) show that young ($<$ 160 Myr) clusters in the Antennae Galaxy have a power-law mass function with index ~ -1 and argue that the power-laws would gradually evolve into log-normal shapes due to dynamical destruction of individual clusters.

Figure 4 shows the mass spectrum of young GCs formed within the preceding 25 Myrs in the middle of the first merger event. It shows a roughly Gaussian shape, with some excess at the high-mass end. If we examine the high-mass tail, there is some hint of power-law behavior, but the slope is steeper than in the Antennae Galaxy. Kravtsov & Gnedin (2003) find a similar Gaussian mass spectrum of young GCs in their cosmological simulations, suggesting that Gaussian-type spectra may

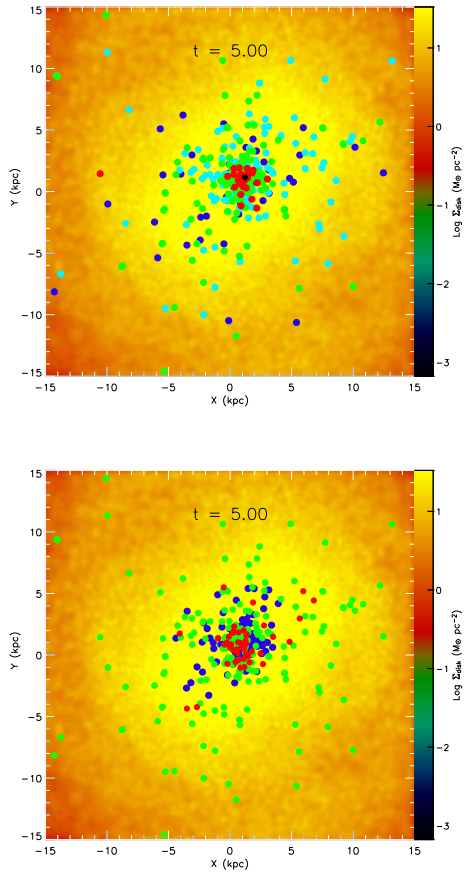

FIG. 3.— Log of stellar surface density in the merger remnant, with values shown in color bar, compared to distribution of GCs (*dots*) in mass (*top panel*) and age (*bottom panel*). Mass bins shown are $M_{\rm gc} < 10^6 M_{\odot}$ (*blue*), $10^6 \leq M_{\rm gc} < 10^{6.5} M_{\odot}$ (*cyan*), $10^{6.5} \leq M_{\rm gc} < 10^7 M_{\odot}$ (*green*), $M_{\rm gc} \geq 10^7 M_{\odot}$ (*red*), and the most massive GC, $M_{\rm gc} = 7.8 \times 10^7 M_{\odot}$ (*black*). Age bins shown are GCs formed at $t < 1.4$ Gyr during initial approach before the merging event begins (*blue*), GCs formed at 1.4 Gyr $< t <$ 1.9 Gyr during the first encounter (*green*), and GCs formed at 4.0 Gyr $< t <$ 4.6 Gyr during the second encounter (*red*).

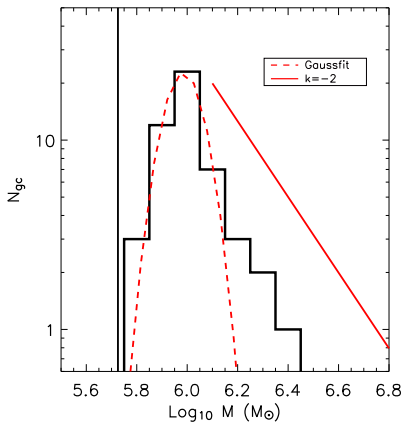

FIG. 4.— Mass spectrum at $t = 1.53$ Gyr of young clusters formed within the preceding 25 Myr. A Gaussian fit to the spectrum (*red dashed line*), and a power law with slope of -2 (*red solid line*) are also shown. The vertical line indicates the mass resolution, defined as twice the kernel mass (Bate & Burkert 1997).

be the signature of gravitational fragmentation, as found, for example, by Klessen & Burkert (2000). However, despite our high resolution, we still cannot resolve the lowest-mass clusters observed in the Antennae Galaxy. If the mass resolution proposed by Bate & Burkert (1997) is an underestimate, the apparent Gaussian peak could be a numerical artifact, perhaps explaining the lack of power-law behavior in our simulation. Higher resolution will be necessary for further investigation. Note we do not include destruction mechanisms such as two-body relaxation (Fall & Zhang 2001) in the simulations, so it is not clear how the spectra evolve over a Hubble time.

6. SUMMARY

We present high-resolution simulations of star cluster formation in both a single galaxy and a major merger, using a three-dimensional SPH code that includes absorbing sink particles to represent massive star clusters. This allows direct identification of individual clusters and tracking of their orbital evolution over several gigayears. The merging galaxies show bursts of massive star cluster formation, in sharp contrast to the steady but slow formation in an isolated galaxy. Most new clusters form in the tidal tails and bridges between the merging galaxies. They are identified as progenitors of globular clusters, although it should be emphasized that these GCs do not lose mass as real ones would due to dynamical effects.

The estimated specific globular cluster frequency $S_{\rm N}$ in the elliptical galaxy resulting from the merger exceeds by a factor of 2.75 that in an isolated galaxy with the same parameters as the merging galaxies. This supports the idea that the higher $S_{\rm N}$ observed in ellipticals is produced by mergers. Clusters formed during different phases of the merging even have distinct radial distributions. The metal-poor old clusters formed before the first encounter as well as the metal-enriched younger clusters from the final merging event are centrally concentrated, while clusters formed in the first encounter are widely distributed. This suggests the observed multimodal metallicity distribution of globular clusters in elliptical galaxies is the direct result of merger processes.

We thank V. Springel for use of both GADGET and his galaxy initial condition generator, as well as for useful discussions. We are grateful for M. Shara for carefully reading the manuscript and helpful suggestions. We also thank A.-K. Jappsen for participating in the implementation of sink particles in GADGET, and K. Bekki, O. Gnedin, and R. McCray for useful discussions. This work was supported by NSF grants AST99-85392 and AST03-07854, NASA grant NAG5-13028, and DFG grant KL1358/1. Computations were performed at the Pittsburgh Supercomputer Center supported by the NSF, on the Parallel Computing Facility of the AMNH, and on an Ultrasparc III cluster generously donated by Sun Microsystems.

REFERENCES

Ashman, K. M., & Zepf, S. E. 1992 ApJ 384, 50
Ashman, K. M., & Zepf, S. E. 1998 Globular Cluster Systems (Cambridge University Press)
Barmby, P. & Huchra, J. P. 2001 AJ 122, 2458
Barnes, J.E. 2002 MNRAS 333,481
Barnes, J.E., & Hernquist, L. 1992 ARA&A 30, 705
Bate, M., Bonnell, I., & Price, N. 1995 MNRAS 277, 362
Bate, M. R. & Burkert, A. 1997 MNRAS 288, 1060
Beasley, M. A. et al. 2002 MNRAS 333, 383
Bekki, K. & Chiba, M. 2002 MNRAS 335, 1176
Bekki, K. et al. 2002 MNRAS 335, 1176
Bromm, V. & Clarke, C. 2002 ApJ 566, 1
Carney, B. W., & Harris, W. E. 2001 Star Clusters (Springer)
Djorgovski, S. & Meylan, G. 1994 ApJ 108, 1292
Dubinski, J., Mihos, C.J., & Hernquist, L. 1999 ApJ 526, 607
Elmegreen, B. G., & Efremov, Y. N. 1997 ApJ 480, 235
Fall, S. M., & Rees, M. J. 1985 ApJ 298, 18
Fall, S. M., & Zhang, Q. 2001 ApJ 561, 751
Farouki, R., & Shapiro, S.L. 1982 ApJ 259, 103
Harris, W. E., 1991 ARA&A 29, 543
Harris, W. E. & Pudritz, R. E. 1994 ApJ 429, 177
Harris, W. E. & van den Berg, S., 1981 AJ 86, 1627
Hernquist, L. 1992 ApJ 400, 460
Holtzman, J.A. et al. 1996 AJ 112, 416
Klessen, R. S., & Burkert, A., 2000 ApJS, 128, 287
Kravtsov, A. V. & Gnedin, O. Y. 2003 astro-ph/0305199
Kundu, A. & Whitmore, B. C. 2001 AJ 121, 2950
Larsen, S. S. et al. 2002 AJ 124, 2615
Li, Y., Mac Low, M.-M. & Klessen, R. S. 2004 in preparation
McLaughlin, D. E. 1999 AJ, 117, 2398
Mengel, S. et al. 2002 A&A 383, 137
Mihos, C.J. & Hernquist, L. 1994 ApJ 427, 112
Mihos, C.J. & Hernquist, L. 1996 ApJ 464, 641
Mo, H. J., Mao, S., & White, S. D. M. 1998 MNRAS 295, 319
Naab, T. & Burkert, A. 2001 ApJ 555, 91
Peebles, P. J. E., & Dicke, R. H. 1968 ApJ 154, 891
Rich, R. M., Shara, M. M. & Zurek, D. 2001 AJ 122, 842
Schweizer, F. et al. 1996 AJ 112, 1839
Springel, V. 2000 MNRAS 312, 859
Springel, V. & White, S. M. D. 1999 MNRAS 307, 162
Springel, V., Yoshida, N. & White, S. D. M. New Astron. 6, 79
Steinmetz, M. & White, S. D. M. 1997 MNRAS 288, 545
Toomre, A., & Toomre J. 1972 ApJ 178, 623
White, S.D.M. 1978 MNRAS 184, 185
Whitmore, B. et al. 1993 AJ 106, 1354
Whitmore, B. & Schweizer, F. 1995 AJ 109, 960
Whitmore, B. et al. 1999 AJ 118, 1551
Whitmore, B. astro-ph/0012546
Whitmore, B. astro-ph/0403709
Zhang, Q. & Fall, S. M. 1999 ApJ 527, 81
Zhang, Q., Fall, S. M. & Whitmore, B. 2001 ApJ 561, 727